



Article

Sustainability Assessment of Second Use Applications of Automotive Batteries: Ageing of Li-Ion Battery Cells in Automotive and Grid-Scale Applications

Andreas Podias ^{1,*}, Andreas Pfrang ^{1,*}, Franco Di Persio ¹, Akos Kriston ¹, Silvia Bobba ², Fabrice Mathieux ² , Maarten Messagie ³ and Lois Boon-Brett ¹

¹ European Commission, Joint Research Centre (JRC), Directorate for Energy, Transport and Climate, Energy Storage Unit, Westerduinweg 3, NL-1755 LE Petten, The Netherlands;

Franco.DI-PERSIO@ec.europa.eu (F.D.P.); Akos.KRISTON@ec.europa.eu (A.K.);

Lois.BRETT@ec.europa.eu (L.B.-B.)

² European Commission, Joint Research Centre (JRC), Directorate for Sustainable Resources, Land Resources Unit, Via E. Fermi 2749, 21027 Ispra, VA, Italy; Silvia.BOBBA@ext.ec.europa.eu (S.B.);

Fabrice.MATHIEUX@ec.europa.eu (F.M.)

³ Vrije Universiteit Brussel, Faculty of Engineering, Department of Electrical Engineering and Energy Technology, Mobility, Logistics and Automotive Technology Research Centre—MOBI, Pleinlaan 2, 1050 Brussels, Belgium; Maarten.Messagie@vub.be

* Correspondence: andreaskmp@hotmail.com (A.P.); andreas.pfrang@ec.europa.eu (A.P.);

Tel.: +31-72-785-0626 (A.P.); +31-22-456-5047 (A.P.)

Received: 4 June 2018; Accepted: 14 July 2018; Published: 18 July 2018



Abstract: The Sustainability Assessment of Second Life Applications of Automotive Batteries (SASLAB) exploratory research project of the European Commission's Joint Research Centre (JRC) aims at developing and applying a methodology to analyse the sustainability of deploying electrified vehicles (xEV) batteries in second use applications. A mapping of industrial demonstration and publicly-funded research projects in the area is presented, followed by an experimental assessment of the capacity and impedance change of lithium-ion cells during calendar and cycle ageing. Fresh cells and cells aged in the laboratory, as well as under real-world driving conditions, have been characterised to understand their application-specific remaining lifetime, beyond the 70% to 80% end-of-first-use criterion. For this purpose, pre-aged cells were examined under duty-cycles that resemble those of second use grid-scale applications.

Keywords: battery calendar life; battery state of health (SoH); cycle life; energy storage; second-life battery

1. Introduction

The commercialisation of xEVs (i.e., all types of electric vehicles (EV): pure battery electric vehicles (BEV), hybrid electric vehicles (HEV), and plug-in hybrid electric vehicles (PHEV)) is accelerating in the global market, in response to global concerns about CO₂ emissions reduction and for energy security. Projected European (EU) sales of new PHEVs and BEVs are expected to reach 0.7–0.8 million in 2020 and 1.65–1.9 million in 2025 [1]. This, in turn, has led to a rapidly increasing demand for high-power and high-energy density traction Li-ion batteries (LIB), and will inevitably translate into an increase of waste xEV batteries after reaching first use end-of-life (EoL) in vehicles. Compliant with the Directive 2000/53/EC on EoL vehicles [2], and the Directive 2006/66/EC on batteries and accumulators and waste batteries and accumulators [3], once collected, batteries are usually recycled. However,

when xEV LIBs no longer meet EV requirements, e.g., when their energy storage capacity has decreased by approximately 20 to 30%, they could be employed in second use applications (see Figure 1), such as within the electrical grid distribution system [4] and/or off-grid applications. The second use of a retired xEV LIB extends its total lifetime value by increasing the economic revenue [5].

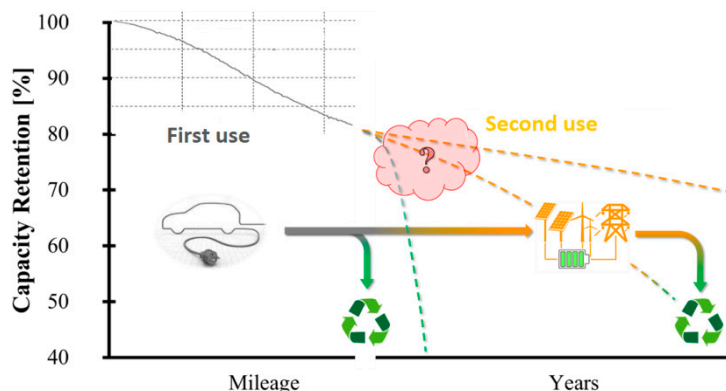


Figure 1. Schematic of degradation during first and second use of an EV battery and scenarios examined within SASLAB: first use + recycling vs. first use + second use + recycling.

In SASLAB, the goal is to study the emerging area of second use application of xEVs batteries and to develop and apply a methodology to analyse the sustainability of such systems. SASLAB particularly aims at better formalising and defining a realistic second use battery system by testing performances of some of its elements (using experimental facilities and physical modelling), and developing relevant performance indicators for the foreseen system (adopting a life cycle thinking approach). Results are evaluated in view of future policy-relevant research needs, considering also economic and social perspectives. The technical feasibility and environmental and economic performances of xEV battery second use need to be assessed, especially considering that the extraction of raw materials used in battery manufacturing and recycling are energy and resource intensive processes [6,7].

This work presents both a mapping of activities/projects/research studies using second life xEV batteries and the experimental assessment of xEV batteries in first and second use applications in terms of capacity and impedance changes during ageing. Ageing, and the state of health (SoH), which characterises the ageing of the battery cells at a defined current rate (C-rate), operating temperature, and state of charge (SoC) (or depth of discharge (DoD)), were analysed using electrochemical impedance spectroscopy (EIS) along with other electrochemical techniques such as incremental capacity analysis (ICA). The results from the experimental assessment are used to develop a comprehensive lifetime model, which provides life-time dependent performance data as the input to life cycle assessment (LCA). The scenarios to be examined within the LCA study are depicted in Figure 1.

2. Mapping of Second Use Activities/Projects/Research Studies

For the purpose of identification of second use applications of xEV batteries, we performed a mapping of international and European industrial demonstration activities, in addition to publicly funded research, development and innovation (RD&I) projects [8]. Furthermore, we reviewed peer-reviewed scientific publications, as well as technical reports by research laboratories, agencies, consultants, and industry analysts [8]. Examples of joint ventures between EV manufacturers and energy companies, and publicly funded RD&I projects are listed in Tables 1 and 2, respectively. The mapping revealed that out of the 35 reviewed activities, applications related to the grid integration of renewable energy (15 out of 35) and to reserve capacity (10 out of 35) are mostly studied [8].

Table 1. Examples of second use storage prototype/pilot/demonstration projects (e.g., joint ventures between EV manufacturers and energy companies)—ten projects in total (see [8]).

EV Company (Project Start)	Energy Company	Project Description
Europe		
BMW (2016)	Vattenfall/Bosch (system integrator)	Pilot energy storage project with a power output of 2 MW and installed capacity of 2.8 MWh. It consists of 2600 modules from over 100 BMW's electric cars (ActiveE and i3 models).
Daimler (2016)	GETEC/The Mobility House Remondis/EnBW	World's largest second use battery storage unit with a total capacity of 13 MWh using EV batteries from Daimler's EVs.
Mitsubishi Motors Corporation/PSA Peugeot Citroën (2015)	Forsee Power/Electricité de France (EDF)/Mitsubishi Corporation	Demonstration project, using battery packs from Peugeot Ion, Citroen C-Zero, and Mitsubishi i-MiEV, to deliver an optimised smart grid and energy management system.
International		
Nissan (2014)	Sumitomo Corporation	Nissan and the Sumitomo Corporation founded 4R Energy Corporation (Yokohama, Japan) in September 2010 as a joint venture to conduct research and repurpose second-life Nissan Leaf battery packs. The world's first large-scale power storage system, a second use prototype system (600 kW/400 kWh) uses 16 Nissan LEAF lithium-ion batteries to test the smoothing effect on the power output from a wind farm in Yume-shima island, Osaka, Japan in 2014.

Table 2. Examples of publicly funded second use storage RD&I projects—seven projects in total (see [8]).

Project Title/Website/Timeframe	Description/Results
Europe	
Batteries2020: Towards realistic EU competitive automotive batteries http://www.batteries2020.eu/ 1 September 2013–31 August 2016	An EU-funded Framework Programme 7 (FP7) project. Assessment of second life post-EV batteries in renewable energy applications took place among other activities. LCA was also conducted to provide an environmental impact of the project-developed prototype lithium nickel manganese cobalt oxide (NMC) cells not only during the manufacturing process, but also during their use in an EV and later during second life and final recycling processes. Two second use applications were considered: (a) a low-demand one [9], with low C-rates and low DoD cycles: a Spanish residential household, which was composed of residential loads, a roof-mounted photovoltaic (PV) system, and a second life battery energy storage system (ESS); and (b) a high-demand application, especially in terms of C-rate, DoD, and number of cycles per year: a second life battery ESS to mitigate the power variability of a grid-scale PV plant [10].
Energy Local Storage Advanced system (ELSA) http://www.elsa-h2020.eu/ 1 April 2015–31 March 2018	An EU-funded Horizon2020 (H2020) project, aiming at enabling the integration of distributed small/medium size storage solutions into the energy system and their commercial use by combining second use batteries with a local ICT-based energy management system. ELSA's ESSs are being applied in six demonstration sites in five EU countries, that include buildings, districts, and distribution grids, covering services such as grid congestion relief, local grid balancing, peak shaving, voltage support, and frequency regulation. Initial results can be retrieved at http://www.elsa-h2020.eu/Results.html .
International	

Table 2. Cont.

Project Title/Website/Timeframe	Description/Results
Battery second use (B2U) United States Department of Energy's (U.S. DoE)/National Renewable Energy Laboratory (NREL) https://www.nrel.gov/transportation/battery-second-use.html 2010-; (ongoing)	The U.S. DoE Vehicle Technologies Office has funded NREL to investigate the feasibility of, and major barriers to the B2U of modern LIBs. NREL suggested that B2U could become an important part of both the automotive and electricity industries. The economic margins that make second use viable are often small; thus several factors could affect this conclusion [5]. Availability of on-board diagnostics data and accurate assessments of automotive and second use battery degradation are considered of outmost importance [4]. Within the B2U project, a methodology and the tools to answer B2U-related questions were developed, including a semi-empirical life model [11] that accounts for both capacity and resistance effects induced by cycling-based and calendar-based mechanisms (nonlinear effects of time, temperature, DoD, and SoC are included), and the Battery Lifetime Simulation Tool (BLAST) [12]. The B2U project has also highlighted the need for additional research and development work to make B2U strategies a reality. NREL is conducting battery life evaluation (in house research), and has partnered with the Center for Sustainable Energy (CSE) and the University of California, San Diego to install a flexible second-use field test bed on a microgrid. CSE studied the baseline health of four EV batteries and developed a long-term testing protocol to track battery performance over time under second use application cycling.

3. Second Use Applications and Duty Cycles

Nowadays, lithium-ion batteries are receiving growing attention as they can be employed to provide one or several services in modern electricity systems [13]. In Germany, according to [14], “the automotive industry is entering into the energy area by offering batteries to both household and commercial users, as well as providing services to utilities and the grid”. It was indicated by [14] that re-purposed (or reconditioned) xEV batteries would be increasingly used in storage applications that can be sited at four levels: off-grid, behind the meter, at the distribution level, or at the transmission level. While there is an added value at all four levels, the behind-the-meter energy storage level is considered the one that can provide the largest number of services to the electricity grid [14,15].

Within SASLAB, the following second use applications were selected for further examination: PV firming (PVF), PV smoothing (PVS), primary frequency regulation (PFR), and peak shaving (PS). These duty cycles (i.e., charge/discharge power profiles that represent the demands placed on an ESS by a specific application), applied to determine the performance of the battery cells in the four mentioned applications, are described in detail in [16–18]. Hereafter, a short description is provided.

Duty cycles for PVF (an energy smoothing) and PVS (a power smoothing) application, as adapted from [16–18], are depicted in Figure 2. The PVS duty cycle is constructed by capturing one-hour “slices” of PV power generation from different days and splicing these slices together into a composite signal of 10 h in length (representing the typical daylight hours of significant PV generation; Figure 2-right), with the majority of these slices representing moderate to very high levels of PV variability. Different times of the day and the year can be captured by one composite signal. The process of constructing the duty PVS cycle signal can be found in [18]. The duty cycle is obtained by normalising the PV power timeseries to the rated power of the smoothing battery (here battery cell) over a 10-h time period, where a positive/negative sign represents discharging power from/charging the battery cell as a function of time in hours. The construction process of the PVF duty cycle (see Figure 2-left) is similar to PVS except that the time windows of interest are in a minutes to hours range, rather than seconds to minutes (for details see [17]).

The PFR duty cycle, as described in detail in [16], consists of three 2-h average standard deviation (SD) power signals, followed by one 2-h high SD (aggressive) signal, three 2-h average SD signals, one 2-h aggressive signal, and four 2-h average SD signals (see Figure 3), with the SD over a 24-h period being the chosen metric for the aggressiveness of the signal analysed (see [16]; the representative 2-h

average and 2-h high SD signals were chosen to compose the duty cycle in such a way that they were energy neutral and had the same SD as the average and aggressive signals over a one-year time frame).

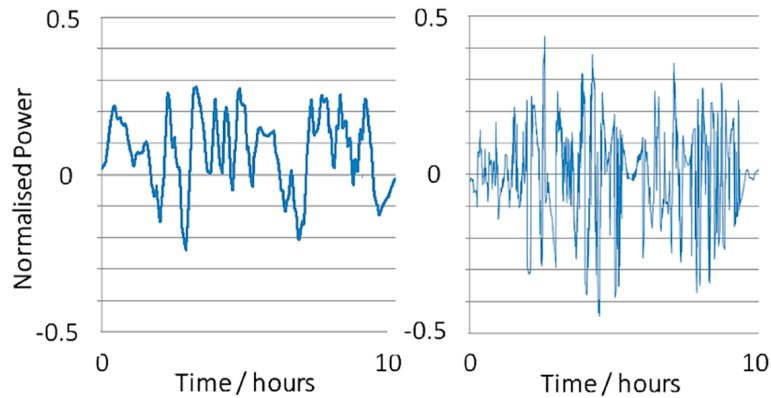


Figure 2. Duty cycles as power normalised by ESS rated power over a 10-h period of time: PVF (left); PVS (right). Adapted from [16–18].

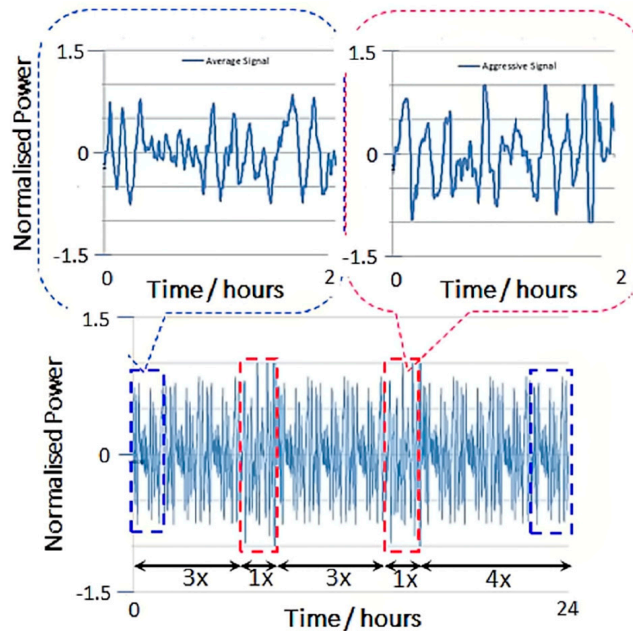


Figure 3. PFR duty cycle as power normalised by ESS rated power. Representative average SD signal (top-left) and representative aggressive SD signal (top-right) over a 2-h period of time (X-axis). PFR duty cycle, composed of three average, one aggressive, three average, one aggressive, and four average signals over a 24-h period of time (bottom); Adapted from [16].

In the PS duty cycles, charge, rest, and discharge time windows (see Figure 4: -1 , 0 , and 1 correspond to charge, rest, and discharge, respectively) are defined. This allows the duty cycle profile to be applied in the same manner to different battery technologies regardless of system size, type, age and condition [16]. As described in [16], each duty cycle has a total charge time of 12 h, the required discharge period duration of 6, 4, and 2 h for duty cycle A, B, and C, respectively (see Figure 4A–C), and a rest (standby) window after charge and discharge that bring the total duration for each of the A, B, and C duty cycles to one 24-h period.

Prior to the test, the battery cell(s) shall be brought to the initial (maximum) SoC by charging at rated power. The test starts with a discharge (duty cycle A) at constant power until the lower SoC limit is reached as specified by the manufacturer, followed by rest (standby), charge at constant power until

the upper SoC limit is reached, rest (standby), and a charge at rated power to bring the cell(s) to the initial (maximum) SoC. Then, duty cycle B and subsequently C follow. Before applying duty cycle B, cell(s) shall be brought to the maximum SoC by charging at rated power; the same holds before applying duty cycle C. Following the application of duty cycle C, the cells shall be brought back to their maximum SoC (or initial SoC if different).

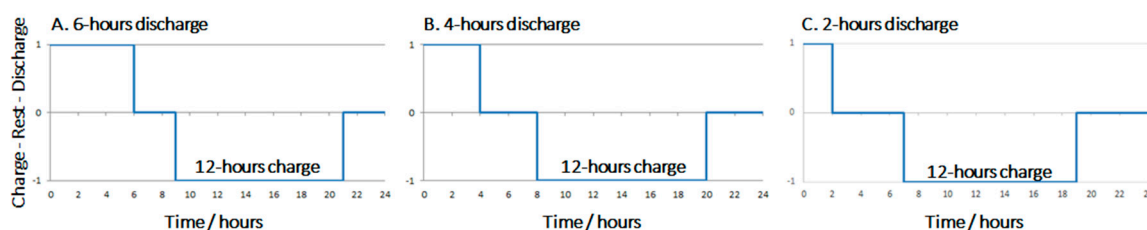


Figure 4. Example of PS duty cycle over a 24 h period of time (X-axis) for each one of the duty cycles (A–C). Charge duration is 12 h. Discharge duration is 6, 4, and 2 h, and rest period is 6, 8, and 10 h for duty cycle A, B, and C respectively.; Adapted from [16].

4. Experimental Assessment of LIB's Ageing in First and Second Use

4.1. Materials and Testing Equipment

The examined LIB cells contain a graphite anode and a composite (blended) cathode, based on lithium manganese oxide (LiMn_2O_4) and lithium nickel manganese cobalt oxide (LiNiMnCoO_2).

Fresh cells (LMO-NMC/graphite; 38 Ah initial rated capacity) and cells aged under real-world driving conditions of the same type, disassembled from the battery pack of a used series-production EV after it had driven 136,877 km (at this point in time, the capacity recorded by the battery management system (BMS) was 30.91 Ah), have been assessed for a better understanding of their extended lifetime, beyond the 70% to 80% capacity EoL criterion. The degradation of the pre-aged LIB cells is also examined under duty cycles that simulate those of second use grid-scale applications (see Figures 2–4). The experimental test rig is depicted in Figure 5.



Figure 5. Battery test rigs: Environmental chambers and cyclers (left, centre); Closer view of EV cells under testing inside the environmental chamber (right).

Aged LMO-NMC/graphite cells were initially screened based on the voltage/temperature recorded by the cell monitoring unit of the EV just before disassembly took place: Three different locations were identified in the battery pack according to the registered temperature. Cells located in location 1 (L1) were at 25 °C, in L2 at 24 °C and in L3 at 23 °C, respectively.

Maccor Series 4000 bidirectional battery testers-cyclers (Maccor, Tulsa, OK, USA) have been used for the ageing studies (current and voltage accuracy: 0.025% and 0.02% of full scale, respectively). These cyclers also control the 12 BiA MTH 4.46 temperature chambers (see Figure 5-centre; BiA, Conflanse Saint Honorine, France) with a temperature accuracy in the centre of the working space of ± 0.5 K and a homogeneity in space relative to the set value of ± 1.5 K (the temperature rate is 2.0 K/min

for both heating and cooling), and the 2 Vötsch VCS3 7060-5 climate chambers (see Figure 5-left; Vötsch Industrietechnik GmbH, Balingen-Frommern, Germany) with a temperature accuracy in the centre of the working space of ± 0.5 K or below and homogeneity in space relative to the set value of ± 2.0 K or better (the temperature rate is 6.0 K/min for both heating and cooling). All temperature (BiA MTH 4.46) and climate chambers (Vötsch VCS3 7060-5) maintain the ambient temperature at a similar specific and constant value (see Table 3). A thermocouple, positioned (and secured) on the cell surface as described in [19], was placed in the centre of one side of each cell to monitor surface temperature variations.

Table 3. Test matrices in (A) calendar and (B) automotive use cycle ageing. Constant current-constant voltage charge/constant current discharge (CC-CV/CC) and Worldwide harmonised Light-duty vehicles Test Cycle (WLTC) protocols were applied for cycle ageing.

(A) Calendar Ageing			(B) Automotive Use Cycle Ageing		
Temperature [°C]	SoC	Cell (Fresh or Aged in EV)	Temperature [°C]	Cycling Profile Charge/Discharge	Cell (Fresh or Aged in EV)
45	100	Aged	45	CC-CV/CC	Fresh
	50	Fresh		CC-CV/CC	Fresh
	50	Aged		WLTC	Fresh
	50	Aged		CC-CV/CC	Aged
	50	Fresh		WLTC	Aged
	100	Fresh		WLTC	Aged
25	100	Aged	25	CC-CV/CC	Fresh
	100	Fresh		WLTC	Fresh
	50	Aged		WLTC	Fresh
	100	Fresh		CC-CV/CC	Aged
	50	Fresh		CC-CV/CC	Aged
	100	Aged		WLTC	Aged

Impedance spectroscopy was carried out using a Maccor FRA 0355 (Maccor, Tulsa, OK, USA) and a ModuLab XM (Solartron Analytical, AMETEK Advanced Measurement Technology, Farnborough, Hampshire, UK).

First (automotive) use cycling utilising the WLTC [20] is performed with a four-channel, BDBT Bidirectional type Battery Test bench (Digatron Power Electronics GmbH, Aachen, Germany), which has a current range of 0 to 200 A (for one channel) and a voltage range of 0 to 100 V. Both the voltage accuracy and the current accuracy are $\pm 0.1\%$ of full scale.

4.2. Ageing Tests

For establishing the experimental procedures applied to the commercial (aged and fresh) LMO-NMC/graphite cells, numerous standards and protocols were consulted. These included standards such as the IEC62660-1 [19], ISO 12405-1 and 2 [21,22], and IEC61427-1 and 2 [23,24], and protocols, such as the one for uniformly measuring and expressing the performance of ESSs, prepared by the Pacific Northwest National Laboratory (PNNL) and Sandia National Laboratories (SNL) [16], and another developed in the EU-funded research project Helios [25].

Test matrices (see Table 3) were devised for testing of the LMO-NMC/graphite cells (fresh and aged under real-world driving conditions) under calendar and cycle ageing, utilising the design of experiments (DOE) methodology, employing the commercial JMP[®] predictive analytics software (SAS, Marlow, Buckinghamshire, UK). These test matrices combine independent variables such as, e.g., temperature, SoC, cell ageing (pre-aged vs. fresh cell), and cycling profile, and were optimised to provide the minimum error of prediction (D-optimised [26]). In this way, maximal information can be retrieved from an optimum number of tests, allowing researchers to evaluate and understand not only the effect of the independent variables on the degradation processes during calendar and cycle (in first and second use) ageing, but also the interactions between them.

Performance degradation during calendar ageing is examined under different temperature and SoC conditions for aged and fresh cells following IEC 62660-1 [19]. For the cycle ageing tests, cells are tested at two constant temperatures (25, 45 °C), under a CC-CV charging/ CC discharging protocol at a specific C-rate, as well as under WLTC and the selected second use duty cycles.

4.3. Performance Tests

Prior to the ageing experiments, cells were placed in a temperature chamber at 25 °C for at least 12 h to ensure thermal equilibrium. Prior to the start of testing and at the end, for all cells undergoing either cycle life testing or calendar life testing, the mass was measured and a reference performance test conducted to determine the baseline and end of test cell performance. Baseline cell performance was subsequently used to assess any changes in the condition of the cell and rate of performance degradation over time and as a function of use.

During ageing tests (see Section 4.2; calendar life, first use and second use cycle life), a set of performance tests is carried out at periodic intervals to establish the condition and rate of performance degradation of cells being tested. The reference performance test includes the quasi-open circuit voltage (quasi-OCV) vs. SoC relationship determination, capacity determination, and EIS (at different SoC: 50% and 100%) determination at 25 °C according to [19]. At defined periodic intervals, every 42 days during calendar life testing, and every 28 days during cycle life (first and second use cycle life) testing, the capacity and EIS tests are repeated to identify how the testing affects cell performance.

The measurement for the quasi-OCV vs. SoC starts with fully charging the cells up to the end-of-charge voltage (EOCV) (4.1 V, as specified by the manufacturer). Then, the cells are discharged to end-of-discharge voltage (EODV) (2.8 V, as specified by the manufacturer) at a C/25 rate (a small enough current rate is utilised for the measured voltage to be considered as “quasi-OCV”). After this step the cell is charged up to the EOCV. The obtained quasi-OCV vs. SoC charging and discharging curves over DoD may differ due to hysteresis effects; thus, their average is considered as the quasi-OCV vs. SoC relationship.

The capacity test consists of charging and discharging steps at 9 A (C/4.22 based on the rated capacity of 38 Ah specified by the manufacturer) at three different temperatures (0 °C, 25 °C and 45 °C). After each charging and discharging step, a sufficient time is included for temperature stabilisation within 1 K/h.

The impedance spectra are measured in galvanostatic mode over a frequency range of 10 kHz to 10 mHz using a Maccor frequency response analyser (FRA) 0355 or 30 kHz to 1 mHz using the ModuLab XM at the respective temperature and SoC, with the FRA equipment being connected to the Maccor cyclers; when FRAs were not connected to the Maccor cyclers, experiments were paused and cells were disconnected from the cyclers for the EIS measurements to take place.

Cell degradation is assessed in terms of capacity retention, impedance growth as tracked via EIS, and incremental capacity analysis (ICA). Incremental capacity (IC) curves are generated utilising post-processed charging/discharging data over lifetime ageing testing. Roundtrip energy efficiency and duty cycle roundtrip efficiency are also determined.

5. Results and Discussion

Nyquist and Bode plots of the impedance of a fresh and a pre-aged cell prior to the start of life testing, thus impedance spectra of cells of different SoH, are depicted in Figure 6. In this test, the impedance spectrum is measured in galvanostatic mode from 30 kHz to 1 mHz (ModuLab XM) at an OCV which corresponds to 50% SoC at room temperature. EIS serves to distinguish electrochemical processes, which can be separated due to different time constants [27,28].

In the Nyquist plot (Figure 6-left), marks A ($|z| = 1.42 \text{ m}\Omega$ at 39.76 Hz), and B ($|z| = 1.81 \text{ m}\Omega$ at 0.39 Hz) for the pre-aged cell, are characteristic points of electrochemical processes, which can be separated due to different time constants. The real part of the impedance crossing the imaginary Y-axis at zero in the Nyquist plot (mark A) is usually mentioned as the ohmic resistance.

The real part of the impedance corresponding to the diameter (resistance at B—resistance at A) (or the sum of diameters in case two semicircles are present) of the envisaged semicircle can be used to quantify the amount of ageing [29], whereas the development of this resistance term can be utilised to assess nonlinear ageing characteristics during prolonged cycling as discussed in [30].

In the Bode plot (Figure 6-right), focusing only on the impedance real part, we notice an impedance increase with ageing between 4 Hz and 1 mHz, which can be explained by a conductivity decrease of the electrolyte due to its decomposition (see e.g., [31]). The degradation of LIBs does not originate from one single cause, however, but from various processes and their interaction. The Bode plot also shows that the greatest influence of ageing is observed in the frequency range below 0.01 Hz to 1 mHz, and especially between 1 Hz to 300 Hz, where degradation is related to the increase of charge transfer and/or solid-electrolyte interphase (SEI) resistance, and changes in double layer capacity (see [32,33] for example descriptions of ageing mechanisms in LIBs).

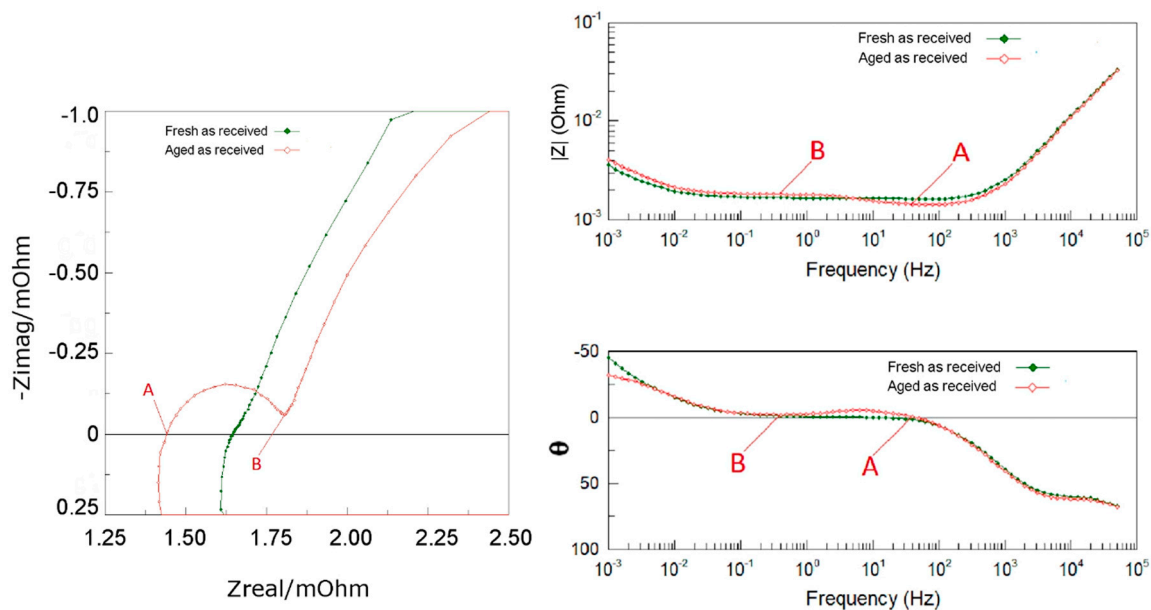


Figure 6. Nyquist (left; data shown only from 60 Hz to 0.009 Hz) and Bode (right; full frequency range) plots of the impedance at an SoC of 50% and at a temperature of 25 °C for the as received fresh and as received pre-aged cells. A and B indicate identical frequencies in the Nyquist and Bode plot (see discussion in the text for the definition of marks A, B in a Nyquist plot).

Figure 7 depicts the impact of calendar life ageing on charge-discharge curves (cell voltage vs. capacity on charge and discharge, and energy on discharge) for a pre-aged LMO-NMC/graphite cell at 45 °C and 100% SoC. Data is shown for four characterisation cycles, recorded with intervals of 42 days, between day 2 and day 135. In general, for a Li-ion cell, one expects the charge behavior to be similar to the discharge behavior at low current rates—this is also the case here, where for the applied current rate, the cell is able to recharge to completion for every characterisation cycle during the calendar life testing so far.

The maximum capacity attained on charge and discharge at the applied current rate is 28.76 Ah and 28.78 Ah, respectively.

Figure 8-left shows the capacity retention of the cell on discharge as a function of the calendar life testing period for an ambient temperature of 45 °C and 100% SoC. After 135 days, the capacity is at 83.38% based on the actual capacity measured in the reference cycle, and 63.53% based on the initial rated capacity of 38 Ah specified by the manufacturer.

The energy content of the cell on discharge (see Figure 8-right) was 92.34 Wh after 135 days (at 81.88% and 64.80% as compared to the reference and the initial rated cell energy content of 142.50 Wh specified by the manufacturer [34], respectively).

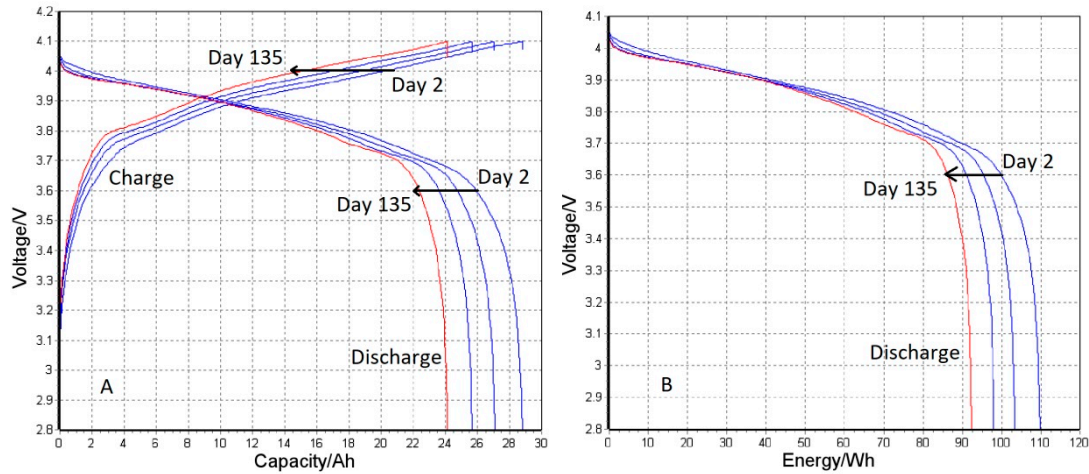


Figure 7. Charge-discharge profiles from reference cycles at C/4.22 (9 A) as a function of calendar ageing (temperature 45 °C, 100% SoC) of a pre-aged LMO-NMC/graphite cell: (A) voltage vs. capacity; (B) voltage vs. energy.

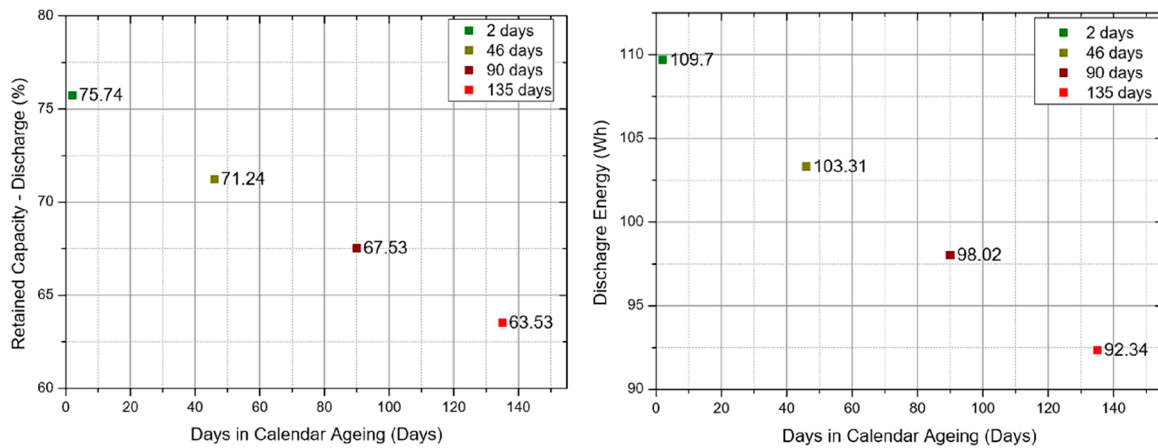


Figure 8. Retained capacity at discharge over calendar ageing (left). Energy at discharge (right) over calendar ageing of a pre-aged LMO-NMC/graphite cell: Temperature 45 °C, 100% SoC.

Nyquist plots of the impedance as a function of ageing obtained in reference tests after two days, 46 days, and 90 days under calendar ageing of a cell at 45 °C and 100% SoC are shown in Figure 9-left. Impedance growth plays a critical role in understanding cell degradation over ageing; we mainly notice that the intercept of the Nyquist plots with the real axis, usually related to ohmic resistances (active materials, current collectors, and electrolyte resistance, also within the separator), is moving to the right (increasing ohmic resistance) with ageing time (see also Figure 9-right). Furthermore, the semicircle at middle frequency (see Figure 9-left) is expanding, representing the increase of charge transfer resistance and/or SEI resistance, as well as changes in double layer capacity.

The degradation, as reflected by the increase of impedance (ohmic resistance) (see Figure 9-right), correlates with the capacity decrease at discharge (see Figure 8-left).

The (differential) ICA depicts capacity change associated with a voltage step (dQ/dV ; with Q being the capacity and V the voltage). It is a technique for observing gradual changes in LIB cells as a function of cell voltage and ageing cycles/days [35,36]. Each peak in the IC curve has a unique

shape, intensity, and position, and it exhibits an electrochemical process taking place in the cell [37]. Even though ICA was originally proposed for ‘close to equilibrium’ conditions—as the ones that have been conducted for the quasi-OCV vs. SoC tests (C/25; results not shown here)—it was shown [38] that the peaks on the IC curve can also be identified with normal charging/discharging data. Hence, indicative results presented hereafter are based on the C/4.22 cell charging/discharging C-rate.

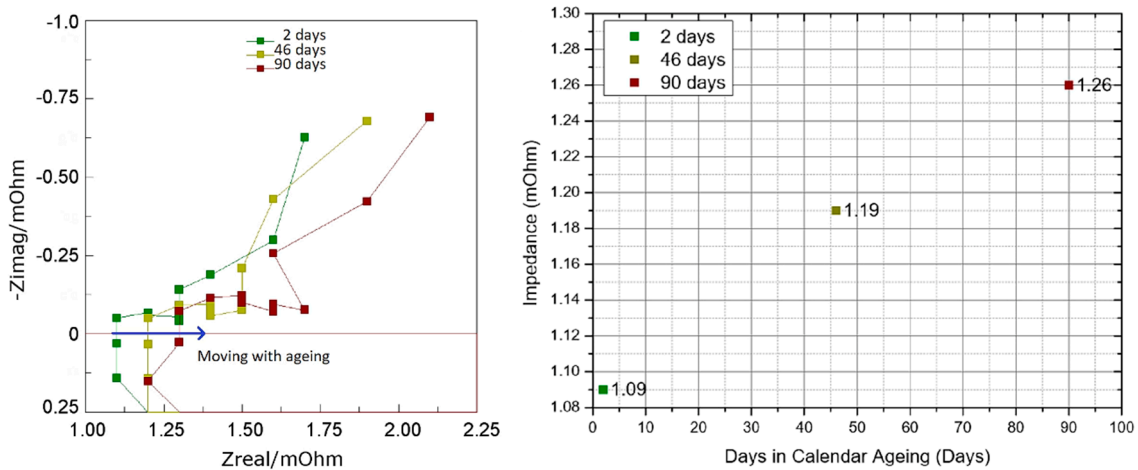


Figure 9. Nyquist plot of impedance spectra (left) and impedance (ohmic resistance) increase (right) of the LMO-NMC/Graphite pre-aged cell over calendar ageing at 45 °C and 100% SoC (data from periodic reference test at 2, 46, and 90 days).

The IC curves of cell charging/discharging data, from the corresponding charge-discharge curves, collected during calendar life testing over 135 days (45 °C, 100% SoC) are shown in Figure 10. The peak heights change with ageing, possibly indicating that the number of available sites for Li occupancy at the respective voltages (or SoC) is changing with ageing [35]. Similar IC curves have been produced for all different ageing conditions utilised in the testing campaign (see Table 3). After quantification of the peak values, they may be correlated with the faded cells’ capacity (results not shown here).

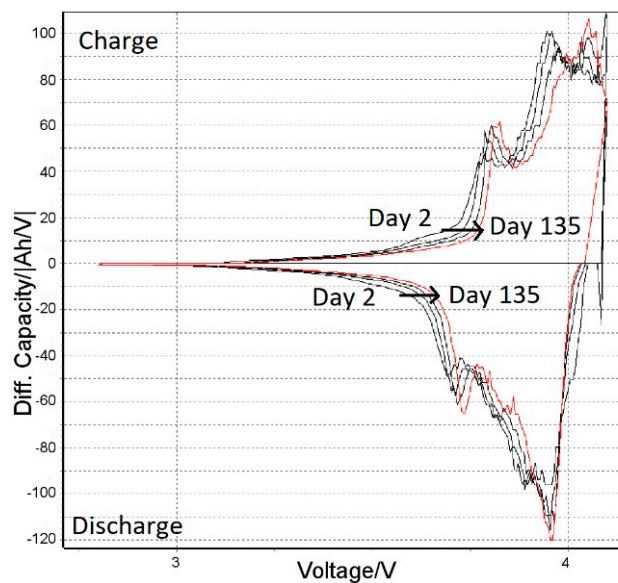


Figure 10. Evolution of the differential capacity vs. voltage curves as a function of calendar ageing of the graphite/LMO-NMC pre-aged cell at 45 °C and 100% SoC (data from periodic reference test at two, 46, 90, and 135 days (red line) in 2.8–4.1 V at the C/4.22 cell charging/discharging C-rate).

6. Conclusions and Outlook

Conservation of resources, along with energy, is becoming more important than ever; therefore, the idea of employing post-EV LIBs originally designed for xEVs to meet the demand for lower intensity stationary storage is gaining acceptance. For enabling this, an accurate assessment of battery degradation in both the automotive and second (stationary) use environments is of utmost importance, to improve understanding and for a better prediction of battery ageing evolution, needed for assessing the economic and environmental benefits of post-EV battery second use.

An experimental campaign has been organised to study the ageing and long-term performance degradation of lithium-ion cells, in terms of capacity and impedance change during calendar and cycle ageing (first and second use cycle life). In addition to automotive drive cycles, such as the WLTC, duty cycles that resemble those of second use grid-scale applications are being utilised (not discussed here). Ageing results were analysed using EIS along with other electrochemical techniques such as ICA.

The work is ongoing and all collected data will help to understand the application-specific remaining lifetime of post-EV cells, beyond the 70% to 80% end-of-first-use criterion, feed into ageing predictive lifetime models, and serve as an input for further LCA analysis. Results of this work (e.g., cycling tests in extended first automotive use and second use applications) will be communicated in forthcoming publications [39–41].

In summary, battery ageing and degradation encounter multiple complex and coupled physicochemical processes in different operating conditions, including dynamic duty cycles, temperature/thermal effects, and other environmental factors. Thus, one of the main challenges for re-using post-EV LIBs in second use applications is to design a BMS able to measure and quantify the evolution of the electrical performances of EV batteries and to use this information for predicting accurately their remaining application-dependent useful life—in both automotive use (1st life) and stationary second use applications (2nd life). As such, information on the application-dependent SoH of the post-EV batteries is necessary [42]. Thus, the identification of a possible correlation between changes in battery capacity and corresponding impedance changes during first (xEV) use and second (stationary) use applications can assist in SoH determination.

Author Contributions: Conceptualization, A.P. (Andreas Podias), A.P. (Andreas Pfrang), F.D.P., A.K., S.B., F.M., M.M.; Methodology, A.P. (Andreas Podias), A.P. (Andreas Pfrang), F.D.P., A.K.; Software, A.P. (Andreas Podias), F.D.P., A.K.; Validation, A.P. (Andreas Podias), F.D.P., A.K.; Formal Analysis, A.P. (Andreas Podias), F.D.P., A.K.; Investigation, A.P. (Andreas Podias), F.D.P., A.K.; Resources, -; Data Curation, -; Writing—Original Draft Preparation, A.P. (Andreas Podias), A.P. (Andreas Pfrang); Writing—Review & Editing, A.P. (Andreas Podias), A.P. (Andreas Pfrang), F.D.P., A.K., S.B., F.M., M.M., L.B.-B.; Visualization, A.P. (Andreas Podias), F.D.P.; Supervision, A.P. (Andreas Pfrang), M.M., L.B.-B.; Project Administration, A.P. (Andreas Pfrang), F.M., L.B.-B.; Funding Acquisition, F.D.P., A.P. (Andreas Pfrang), F.M., L.B.-B.

Funding: This research received no external funding.

Acknowledgments: This work is part of the in-house Exploratory Research project SASLAB of the European Commission's JRC. The thorough review of the manuscript by Marc Steen (JRC) is kindly acknowledged.

Conflicts of Interest: The authors declare no conflicts of interest.

References

1. Lebedeva, N.; Di Persio, F.; Boon-Brett, L. *Lithium Ion Battery Value Chain and Related Opportunities for Europe*; European Commission: Petten, The Netherlands, 2016.
2. Directive 2000/53/EC on End-of-Life Vehicles. Available online: http://ec.europa.eu/environment/waste/elv/legislation_en.htm (accessed on 17 April 2017).
3. Directive 2006/66/EC on Batteries and Accumulators and Waste Batteries and Accumulators and Repealing Directive 91/157/EEC. Available online: <http://ec.europa.eu/environment/waste/batteries/legislation.htm> (accessed on 17 April 2017).
4. Neubauer, J.; Wood, E.; Pesaran, A. A Second Life for Electric Vehicle Batteries: Answering Questions on Battery Degradation and Value. *SAE Int. J. Mater. Manuf.* **2015**, *8*, 21–23. [CrossRef]

5. Neubauer, J.; Pesaran, A. The ability of battery second use strategies to impact plug-in electric vehicle prices and serve utility energy storage applications. *J. Power Sources* **2011**, *196*, 10351–10358. [[CrossRef](#)]
6. Oliveira, L.; Messagie, M.; Rangaraju, S.; Sanfelix, J.; Hernandez Rivas, M.; Van Mierlo, J. Key issues of lithium-ion batteries—From resource depletion to environmental performance indicators. *J. Clean. Prod.* **2015**, *108*, 354–362. [[CrossRef](#)]
7. Peters, J.F.; Weil, M. A Critical Assessment of the Resource Depletion Potential of Current and Future Lithium-Ion Batteries. *Resources* **2016**, *5*, 46. [[CrossRef](#)]
8. Podias, A.; Bobba, S.; Di Persio, F.; Messagie, M.; Tecchio, P.; Mathieux, F.; Pfrang, A. *Sustainability Assessment of Second Life Applications of Automotive Batteries (SASLAB)*; Exploratory Research Intermediate Report 2016; European Commission: Petten, The Netherlands, 2017.
9. Saez-de-Ibarra, A.; Martinez-Laserna, E.; Koch-Ciobotaru, C.; Rodriguez, P.; Stroe, D.-I.; Swierczynski, M. Second life battery energy storage system for residential demand response service. In Proceedings of the 2015 IEEE International Conference on Industrial Technology (ICIT), Seville, Spain, 17–19 March 2015; pp. 2941–2948.
10. Koch-Ciobotaru, C.; Saez-de-Ibarra, A.; Martinez-Laserna, E.; Stroe, D.-I.; Swierczynski, M.; Rodriguez, P. Second life battery energy storage system for enhancing renewable energy grid integration. In Proceedings of the 2015 IEEE Energy Conversion Congress and Exposition (ECCE), Montreal, QC, Canada, 20–24 September 2015; IEEE: New York, NY, USA, 2015; pp. 78–84.
11. Smith, K.; Earleywine, M.; Wood, E.; Neubauer, J.; Pesaran, A. *Comparison of Plug-In Hybrid Electric Vehicle Battery Life across Geographies and Drive Cycles*; SAE Technical Paper 2012-01-0666; SAE: Detroit, MI, USA, 2012.
12. Neubauer, J. Battery Lifetime Analysis and Simulation Tool (BLAST) Documentation, NREL/TP-5400-63246, December 2014. Available online: <http://www.nrel.gov/docs/fy15osti/63246.pdf> (accessed on 16 December 2016).
13. DOE Global Energy Storage Database, Sandia National Laboratories. Available online: <http://www.energystorageexchange.org/projects> (accessed on 16 December 2016).
14. Reid, J.; Julve, G. Second Life-Batteries as Flexible Storage for Renewables Energies, Report Commissioned by the Federal Association for Renewable Energy (BundesverbandesErneuerbareEnergie e.V.) and the Hanover Fair (Hannover Messe), Berlin, Germany, April 2016. Available online: https://www.bee-ev.de/fileadmin/Publikationen/Studien/201604_Second_Life-Batterien_als_flexible_Speicher.pdf (accessed on 23 September 2016).
15. Fitzgerald, G.; Mandel, J.; Morris, J.; Hervé, T. *The Economics of Battery Energy Storage: How Multi-Use, Customer-Sited Batteries Deliver the Most Services and Value to Customers and the Grid*; Rocky Mountain Institute (RMI): Snowmass, CO, USA, 2015. Available online: http://www.rmi.org/electricity_battery_value (accessed on 23 September 2016).
16. Conover, D.R.; Crawford, A.J.; Fuller, J.; Gourisetti, S.N.; Viswanathan, V.; Ferreira, S.R.; Schoenwald, D.A.; Rosewater, D.M. Protocol for Uniformly Measuring and Expressing the Performance of Energy Storage Systems, PNNL-22010 Rev 2/SAND2016-3078 R, Pacific Northwest National Laboratory, and Sandia National Laboratories, Richland, Washington, and Albuquerque. New Mexico (USA), April 2016. Available online: <http://www.sandia.gov/ess/publications/SAND2016-3078R.pdf> (accessed on 16 December 2016).
17. Schoenwald, D.; Ellison, J. Determination of Duty Cycle for Energy Storage Systems in a Renewables (Solar) Firming Application, SAND2016-3636, Sandia National Laboratories, Albuquerque, New Mexico 87185 and Livermore, California 94550 (USA), April 2016. Available online: <http://www.sandia.gov/ess/publications/SAND2016-3636.pdf> (accessed on 16 December 2016).
18. Schoenwald, D.; Ellison, J. Determination of Duty Cycle for Energy Storage Systems in a PV Smoothing Application, SAND2016-3474, Sandia National Laboratories, Albuquerque, New Mexico 87185 and Livermore, California 94550 (USA), April 2016. Available online: <http://www.sandia.gov/ess/publications/SAND2016-3474.pdf> (accessed on 16 December 2016).
19. International Standard IEC 62660-1:2010. *Secondary Lithium-Ion Cells for the Propulsion of Electric Road Vehicles—Part 1: Performance Testing*; IEC: Geneva, Switzerland, 2010; ISBN 978-2-88912-308-7.
20. Tutuianu, M.; Marotta, A.; Steven, H.; Ericsson, E.; Haniu, T.; Ichikawa, N.; Ishii, H. Development of a Worldwide Harmonized Light-Duty Vehicles Driving Test Cycle (WLTC), Tech. Report,

- UN/ECE/WP.29/GRPE/WLTP-IG, DHC Subgroup. 2013. Available online: <https://www.unece.org/fileadmin/DAM/trans/doc/2014/wp29grpe/GRPE-68-03e.pdf> (accessed on 16 December 2016).
21. International Standard ISO 12405-1. *Electrically Propelled Road Vehicles—Test Specification for Lithium-Ion Battery Packs and Systems—Part 1: High-Power Applications*; IEC: Geneva, Switzerland, 2010.
 22. International Standard ISO 12405-2. *Electrically Propelled Road Vehicles—Test Specification for Lithium-Ion Battery Packs and Systems—Part 2: High-Energy Applications*; IEC: Geneva, Switzerland, 2010.
 23. International Standard IEC 61427-1. *Secondary Cells and Batteries for Renewable Energy Storage—General Requirements and Methods of Test—Part 1: Photovoltaic off-Grid Application*, 1st ed.; IEC: Geneva, Switzerland, 2013; ISBN 978-2-83220-763-5.
 24. International Standard IEC 61427-2. *Secondary Cells and Batteries for Renewable Energy Storage—General Requirements and Methods of Test—Part 2: On-Grid Applications*, 1st ed.; IEC: Geneva, Switzerland, 2015; ISBN 978-2-8322-2881-4.
 25. Mettlach, H.; Delcorso, F.; Gosso, M.; Warm, A.; Porcellato, D.; Bryngelsson, H.; Sarrazin, C.; Conte, M.; Binotto, C.; Doering, H. Initial Cycling & Calendar Ageing Test Procedures and Checkup Tests for High Energy Li-Ion Battery Cells, Project HELIOS—High Energy Lithium-Ion Storage Solutions—Cell Test Specification, October 2012. Available online: www.helios-eu.org (accessed on 23 September 2016).
 26. Atkinson, A.C.; Donev, A.N.; Tobias, R.D. *Optimum Experimental Designs, with SAS*; Oxford University Press: Oxford, UK, 2007; ISBN 978-0-19-929660-6.
 27. Stoyanov, Z.; Grafov, B.; Savova-Stoyanova, B.; Elkin, V. *Electrochemical Impedance*; Publishing House Science: Moscow, Russia, 1991.
 28. Barsukov, E.; Ross Macdonald, J. *Impedance Spectroscopy: Theory, Experiment, and Applications*, 2nd ed.; Wiley-Interscience: New York, NY, USA, 2005.
 29. Schuster, S.F.; Bach, T.; Fleder, E.; Muller, J.; Brand, M.; SEXTL, G.; Jossen, A. Nonlinear aging characteristics of lithium-ion cells under different operational conditions. *J. Energy Storage* **2015**, *1*, 44–53. [[CrossRef](#)]
 30. Burns, J.C.; Kassam, A.; Sinha, N.N.; Downie, L.E.; Solnickova, L.; Way, B.M.; Dahn, J.R. Predicting and Extending the Lifetime of Li-ion Batteries. *J. Electrochem. Soc.* **2013**, *160*, A1451–A1456.
 31. Wright, R.B.; Motloch, C.G.; Belt, J.R.; Chrostophersen, J.P.; Ho, C.D.; Richardson, R.A.; Bloom, I.; Jones, S.A.; Battaglia, V.S.; Henriksen, G.L.; et al. Calendar- and cycle-life studies of advanced technology development program generation 1 lithium-ion batteries. *J. Power Sources* **2002**, *110*, 445–470. [[CrossRef](#)]
 32. Wohlfahrt-Mehrens, M.; Vogler, C.; Garche, J. Aging mechanisms of lithium cathode materials. *J. Power Sources* **2004**, *127*, 58–64. [[CrossRef](#)]
 33. Vetter, J.; Novak, P.; Wagner, M.R.; Veit, C.; Moeller, K.-C.; Besenhard, J.O.; Winter, M.; Wohlfahrt-Mehrens, M.; Vogler, C.; Hammouche, A. Ageing mechanisms in lithium-ion batteries. *J. Power Sources* **2005**, *147*, 269–281. [[CrossRef](#)]
 34. Lithium Energy Japan. *Safety Data Sheet LEV40-8 Lithium-Ion Battery*; D Revision; Lithium Energy Japan: Ritto, Japan, 2016.
 35. Dubarry, M.; Svoboda, V.; Hwu, R.; Liaw, B.Y. Incremental Capacity Analysis and Close-to-Equilibrium OCV measurements to quantify capacity fade in commercial rechargeable lithium batteries. *Electrochem. Solid-State Lett.* **2006**, *9*, A454–A457. [[CrossRef](#)]
 36. Smith, A.J.; Dahn, J.R. Delta Differential Capacity Analysis. *J. Electrochem. Soc.* **2012**, *159*, A290–A293. [[CrossRef](#)]
 37. Dubarry, M.; Liaw, B.Y. Identify capacity fading mechanism in a commercial LiFePO₄ cell. *J. Power Sources* **2009**, *194*, 541–549. [[CrossRef](#)]
 38. Weng, C.; Cui, Y.; Sun, J.; Peng, H. On-board state of health monitoring of lithium-ion batteries using incremental capacity analysis with support vector regression. *J. Power Sources* **2013**, *235*, 36–44. [[CrossRef](#)]
 39. Bobba, S.; Pfrang, A.; Ardente, F.; Blengini, G.A.; Podias, A.; Mathieux, F.; Cusenza, M.A. Life Cycle Assessment of repurposed electric vehicles batteries: An adapted method based on modelling of energy flows. *J. Energy Storage* **2018**. accepted.
 40. Cusenza, M.A.; Bobba, S.; Ardente, F.; Cellura, M.; Di Persio, F. Energy and environmental assessment of a traction lithium-ion battery pack for plug-in hybrid electric vehicles. *J. Clean. Prod.* **2018**. under review.

41. Bobba, S.; Podias, A.; Di Persio, F.; Messagie, M.; Tecchio, P.; Cusenza, M.A.; Eynard, U.; Mathieux, F.; Pfrang, A. *Sustainability Assessment of Second Life Applications of Automotive Batteries (SASLAB)*; Final Technical Report; European Commission: Petten, The Netherlands, 2018.
42. Chiang, Y.-H.; Sean, W.-Y.; Ke, J.-C. Online estimation of internal resistance and open-circuit voltage of lithium-ion batteries in electric vehicles. *J. Power Sources* **2011**, *196*, 3921–3932. [[CrossRef](#)]



© 2018 by the authors. Licensee MDPI, Basel, Switzerland. This article is an open access article distributed under the terms and conditions of the Creative Commons Attribution (CC BY) license (<http://creativecommons.org/licenses/by/4.0/>).